Humidity Sensor Circuits Based on the Current Processing

Predrag B. Petrović, Marija-Vesna Nikolić , Mihajlo Tatović

***Abstract*—A novel electronic conditioning circuits based on the current-processing technique for accurate and reliable humidity measurement, without post-processing requirements, are presented. The pseudobrookite nanocrystalline (Fe_2TiO_5) thick film was used as capacitive humidity transducer in proposed design. The interface circuitry was realized in TSMC 0.18µm CMOS technology. The sensing principle of the sensor was obtained by converting the information on environment humidity into a frequency variable square-wave current signal. The proposed solution features high linearity, insensitivity to temperature, as well as low power consumption. The sensor has a linear function with relative humidity in the range of Relative Humidity (RH) 30-90%, error below 1.5% and sensitivity 8.3 x1014Hz/F evaluated over the full range of change. A fast recovery without the need of any refreshing methods was observed with a change in RH. The total power dissipation of readout circuitry was 1mW.**

***Index Terms*—Current-processing, humidity sensor, CMOS integrated circuit.**

I. Introduction

HUMIDITY sensors have a wide application in everyday practice, including agriculture, monitoring climate change, food storage processes and in the operation of various home appliances [1, 2]. In order to meet the demands of such applications, humidity sensors should provide high sensitivity and linearity in response, in a wide range of possible changes in processed humidity under different temperature conditions. In addition to the aforementioned demands, the sensor circuits must provide long-term stability, short response times with low energy consumption. There are different types of humidity sensors in accordance with the physical principle used to make the conversion: resistive, mechanical, gravimetric, capacitive and thermal humidity sensors [3]. Most electronic circuits, representing the interface between the sensor itself and the processor unit, are based on the use of operational amplifiers [4]. The growing desire for miniaturization of such systems and reduction of their consumption places increasing challenges in the design process before the circuit designers. CMOS technology is a logical response to such challenges, but due to the different ratio of the width and length (W/L) of the transistors used, there is a trade-off between the speed, gain, power and other parameters [5]. The sensor circuit has often been based on the principle of a resistor sensor [6]. Such sensors can detect changes in temperature, humidity, pressure, etc. The capacitive sensor on the other hand can process moisture, speed, and acoustic shift and so on. Sensing circuits that detect the change of resistance enable a relatively simple realization of the accompanying electronic interface.

Everything listed was the reason for the development of the sensor circuit suggested in this paper. Metal oxide semiconductor materials have been intensively investigated for application as humidity sensors [7, 8]. The humidity sensing mechanism of metal oxides is simple. It is based on water adsorption on the material surface that is composed of grains, grain boundaries and pores. Nanostructures and nanomaterials have led to many new applications of metal oxides due to changing and enhancing their microstructural properties [9]. Pseudobrookite (Fe_2TiO_5) is an iron titanium oxide, with a band gap similar to hematite with potential for application as a gas sensor. We have investigated possible application of pseudobrookite for NO gas sensing [10], but our recent work has focused on humidity sensing properties of this material [11].

Analogue interface circuits used in capacitive sensors are based on the application of one of the following methods: measurement based on the application of AC sources to detect the voltage and current at unknown capacitance; using a capacitance divider; resonance and bridge circuits containing the measured capacity; methods based on charge transfer; differential methods [2, 12].

This paper proposes a cheap, accurate, and reliable humidity sensor by integrating the sensing element and the conditioning circuits using standard CMOS technology for fabrication. We propose a new electronic interface circuit based on the concept of current mode processing, which is capable of converting information on environment humidity to variable frequency dependency current (or voltage) signals. To do this we used only one active element, DXCCTA- dual-X current conveyor transconductance amplifiers. Application of this active element is dictated by characteristics of the sensor element-pseudobrookite, and its equivalent impedance circuits.

Practically, design of interface electronic circuits is the central and completely new part of the paper, because all other parts are based on known configurations, not used up till now for practical realization of a humidity sensor. DXCCTA not used until now as the base component for realization of square-wave signals-converter of moisture to time depended

This work was supported in part by the projects OI 172057, 42009 and III45007, funded by the Ministry of Education, Science and Technological Development of the Republic of Serbia.

P. B. Petrović is with the Facuty of Technical Sciences, University of Kragujevac, 32000 Čačak, Serbia (e-mail: predrag.petrovic@ftn.kg.ac.rs).

M. V. Nikolić, was with Institute for Multidisciplinary Research, University of Belgrade, 11000 Belgrade, Serbia (e-mail: mariav@rcub.bg.ac.rs).

M. Tatović is with the Facuty of Technical Sciences, University of Kragujevac, 32000 Čačak, Serbia (e-mail: mihajlo.tatovic@ftn.kg.ac.rs).

current signal. We created a system for checking humidity information in real time. Moreover, the use of grounded passive components in circuit implementation is also beneficial from the integration point of view.

The proposed conditioning circuit was verified through the HSPICE simulation results carried using 0.18 μm CMOS technology, and can operate very well with nonlinearity less than 1%. This technology is a strong candidate for the easy-to-scale implementation of next generation electronics, such as the Internet of things (IoT) [13], LoRa-based sensor technology (for example the RN2483 LoRa transceiver module), built around a Semtech SX1276 transceiver [14], and printed passive/active electronics.

II. Proposed Electronic Interface Circuits

We used a newly proposed active element, DXCCTA as the base for the realization of the interface between the transducer and acquisition unit (for example, microcontroller PIC 18F45K80, a high performance 8-bit MCU [16]), Fig 1a. Practically, DXCCTA is a combination of two versatile active elements: DXCCII and an operational transconductance amplifier (OTA), with electronic tunability capability [16]. Thus, DXCCTA enjoys all the benefits of DXCCII and OTA, but they have never been used in realization of a sensor circuit. Some applications require an extra buffer in the active element to meet the requirement of an appropriate impedance level for the output signal [12]. This is not the case with our proposed sensor circuits, because we select port connections in a new and appropriate way. Fig. 1b shows CMOS implementation of the used DXCCTA.

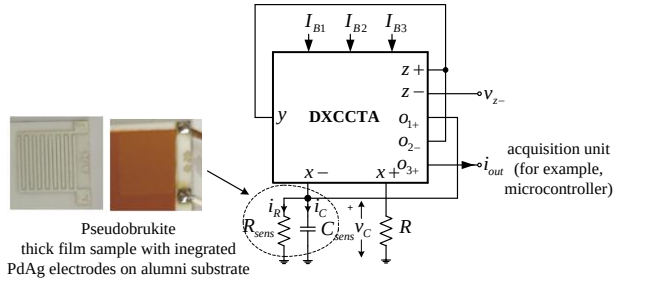

(a)

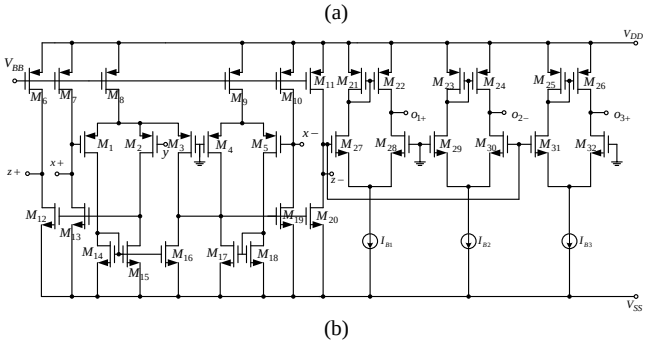

(b)

Fig. 1. (a) Circuit of the proposed conditioning-interface circuits, (b) CMOS implementation of DXCCTA.

As we can see, DXCCTA has eight terminals of which *x+* and *x-* terminals are low impedance terminals whereas the terminals *y*, *z+*, *z-*, *o1+*, *o2-* and *o3+* are high impedance terminals. In CMOS implementation of DXCCTA, Fig. 1b, MOS transistors, M1-M20 form sub-block DXCCII, and MOS transistors, M21-M32 form OTA stages.

Detailed operation of DXCCTA in the saturation region is given in [16], and this operation mode is further utilized in operation of the proposed sensor circuit. The proposed humidity to frequency converter (Fig. 1a) comprises of a single DXCCTA, one grounded resistor and grounded humidity transducer, which we can equivalent represent as parallel connection of resistor and capacitor, R_{sens} and C_{sens} (transducer equivalent impedances). The output current mode square wave, i_{out} is explicitly available from the high impedance terminal, o_{3+}. Fig. 1a shows that terminal *z-* is floated, therefore the voltage, v_{z-} saturates either to V_{DD} or V_{SS} depending on the current i_{z-}. The voltage, v_{z-} in saturation mode is expressed as follows (1).

$$v_{z-} = \begin{cases} V_{DD} \ \ for\ i_{z-} \geq 0 \\ V_{SS} \ \ for\ i_{z-} < 0 \end{cases} \tag{1}$$

These levels of v_{z-} are high enough to saturate all OTAs and currents, i_{o1+}, i_{o2-} and i_{o3+} become totally dependent on bias currents of their respective OTA stage as per (2). The two saturation levels of i_{out} are I_{B3} and $-I_{B3}$. The duration of intervals in which this square wave current signal follows this saturation levels depend on the voltage dynamics across the sensor equivalent circuit. The threshold levels are V_{HT} (higher-upper threshold) and V_{LT} (lower threshold), and they are defined with a bias current I_{B2} and external resistance R. The operation of the proposed circuit can be described as follows: Suppose initially i_{out} is at its positive saturation level, I_{B3}. At the same time i_{o1+} and i_{o2-} will be I_{B1} and $-I_{B2}$, respectively. The current, i_{o1+} causes the capacitor to charge with the following dynamics:

$$i_{Csens}(t) = \frac{v_{Csens}(t)}{R_{sens}} + C_{sens}\frac{dv_{Csens}(t)}{dt}, 0 \leq t \leq T_{ON} \tag{2}$$

$$\Rightarrow R_{sens}C_{sens}\frac{dv_{Csens}(t)}{dt} + v_{Csens}(t) = I_{B1}R_{sens}$$

The limiting values of voltage across the sensor were defined with the threshold level V_{HT} of the v_{x+}. When v_{x+} becomes just higher than the level V_{HT}, the sum of currents i_{z+} and i_{o2-} becomes negative causing the v_{z-} to saturate to V_{SS}. Therefore, i_{out} is now changed to $-I_{B3}$ from positive saturation level, I_{B3}. Thus, i_{o1+} and i_{o2-} are now changed to $-I_{B1}$ and I_{B2}, respectively. A negative current, $-I_{B1}$ at terminal, o_{1+} causes the sensor to discharge with the above defined dynamics until v_{x+} reaches the threshold level V_{LT}. When v_{csens} becomes just less than V_{LT}, the sum of currents i_{z+} and i_{o2-} becomes positive causing v_{z-} to saturate to V_{DD} and i_{out} is again changed to I_{B3}. The amplitude of i_{out} is expressed as

$$i_{out} = \begin{cases} I_{B3} \ \ for\ v_{z-} = V_{DD} \\ -I_{B3} \ \ for\ v_{z-} = V_{SS} \end{cases} \tag{3}$$

The threshold levels of v_{x+} and the peak to peak amplitude, $v_{x+(p\text{-}p)}$ are given as

$$V_{HT} = I_{B2}R \ and \ V_{LT} = -I_{B2}R$$
$$v_{x+(p-p)} = V_{HT} - V_{LT} = 2I_{B2}R \tag{4}$$

The on and off time periods (T_{ON} and T_{OFF}, respectively) are obtained from voltage across the sensor (their waveforms) by comparing the slope during these two time periods

$$v_{Csens}(t) = I_{B1}R_{sens}\left(1-e^{-t/\tau}\right)+V_{TL}e^{-t/\tau}, \tau = R_{sens}C_{sens}$$
$$\Rightarrow V_{TH} = I_{B1}R_{sens}\left(1-e^{-T_{ON}/\tau}\right)+V_{TL}e^{-T_{ON}/\tau}$$
$$\Rightarrow T_{ON} = \tau \ln\frac{V_{TL}-I_{B1}R_{sens}}{V_{TH}-I_{B1}R_{sens}} = \tau \ln\frac{I_{B2}R+I_{B1}R_{sens}}{I_{B1}R_{sens}-I_{B2}R} \quad (5)$$

During the off time period, the voltage across the sensor will be change with the following dynamics:

$$R_{sens}C_{sens}\frac{dv_{Csens}(t)}{dt}+v_{Csens}(t) = -I_{B1}R_{sens}, T_{ON} \le t \le T_{ON}+T_{OFF} = T$$
$$\Rightarrow v_{Csens}(t) = I_{B1}R_{sens}\left(e^{-(t-T_{ON})/\tau}-1\right)+V_{TH}e^{-(t-T_{ON})/\tau}, v_{Csens}(T_{ON}+T_{OFF}) = V_{TL} \quad (6)$$
$$\Rightarrow T_{OFF} = \tau \ln\frac{V_{TH}+I_{B1}R_{sens}}{V_{TL}+I_{B1}R_{sens}} = \tau \ln\frac{I_{B2}R+I_{B1}R_{sens}}{I_{B1}R_{sens}-I_{B2}R}$$

From (6), it is noted that both cycle periods are equal thus the duty cycle of the generated square current signal on port o_{3+} is fixed to 50%. The oscillation frequency, f_0 is obtained from T_{ON} and T_{OFF} as follows

$$f_o = \frac{1}{T_{ON}+T_{OFF}} = \frac{1}{2R_{sens}\,C_{sens}\ln\frac{I_{B2}R+I_{B1}R_{sens}}{I_{B1}R_{sens}-I_{B2}R}} \quad (7)$$

It is observed from (3) and (7) that the amplitude of i_{out} and oscillation frequency, f_0 are electronically and independently tunable via bias currents, I_{B3} and I_{B1}, respectively. Also, the period of the generated square wave current output signal directly depends on parameters of sensor circuits. This way we come into the position to indirectly recalculate the humidity of the environment in which we place our sensor from information on the generated frequency of the current output signal. The generated output signal is completely autonomous and its frequency has no effect on the capacitance of the sensor, which is very often seen in the so far known interface circuit realizations [17], in which the detection of moisture is based on the principle of moisture adsorption and desorption.

The performance of the proposed circuits can be further evaluated based on the sensitivity of its response relative to the sensors parameters C_{sens} and R_{sens}. Sensitivity (S) is defined as an incremental change in the output signal value relative to the incremental change in the sensor parameter [18]. According to such a criterion, the sensitivity of the analysed circuit for the interface is obtained as:

$$S_{C_{sens}} = \frac{\partial f_0}{\partial C_{sens}} = -\frac{1}{2R_{sens}\,C_{sens}^2\ln\frac{I_{B2}R+I_{B1}R_{sens}}{I_{B1}R_{sens}-I_{B2}R}}$$
$$S_{R_{sens}} = \frac{\partial f_0}{\partial R_{sens}} = \frac{\frac{I_{B1}I_{B2}RR_{sens}}{(I_{B2}R+I_{B1}R_{sens})(I_{B1}R_{sens}-I_{B2}R)}-\ln\frac{I_{B2}R+I_{B1}R_{sens}}{I_{B1}R_{sens}-I_{B2}R}}{2R_{sens}^2\,C_{sens}\ln^2\frac{I_{B2}R+I_{B1}R_{sens}}{I_{B1}R_{sens}-I_{B2}R}} \quad (8)$$

Based on the obtained relations (8), the sensitivity can be adjusted by properly selecting the values of the parameters, and for measured values (section IV) we can conclude that the proposed circuits offer satisfactory low sensitivity.

A. Humidity Transducer

The pseudobrookite humidity transducer was developed by screen printing thick film paste on alumina substrate with test interdigitated PdAg electrodes. This design is simple, and is commonly applied for sensing [19]. Pseudobrookite powder and thick film paste was synthesized and characterized in detail and this is described [11]. Interdigitated PdAg electrodes were first screen printed on alumina substrate and fired in a conveyer furnace at 850ºC for 10 minutes in air [11]. The electrode dimensions were: width 8mm, length 8mm, electrode spacing 0.25 mm (Fig. 1a). Five layers of pseudobrookite thick film paste were then screen printed on the substrate with electrodes, with the procedure described in detail in [11] achieving a porous nanocrystalline thick film layer about 60 μm thick (as each layer was~12 μm).

The influence of the change in relative humidity (RH) 30-90% of several thick film pseudobrookite sensors on complex impedance were monitored in a humidity chamber and analysed in detail in [11]. The response and recovery times were relatively rapid (16 s) and relatively low hysteresis (difference between absorption and desorption) were obtained showing that pseudobrookite thick film sensors are good candidates for application in humidity sensing.

III. Estimation of the Influences of Non-idealites and Effects on Measurement Accuracy

In a non-ideal case the terminal characteristics of DXCCTA can be described in the following manner

$$v_{x+} = \beta_1 v_y, v_{x-} = -\beta_2 v_y, i_{z+} = \alpha_1 i_{x+}, i_{z-} = \alpha_2 i_{x-},$$
$$i_{o1+} = \gamma_1 g_{m1} v_{z-}, i_{o2-} = -\gamma_2 g_{m2} v_{z-}, i_{o3+} = \gamma_3 g_{m3} v_{z-} \quad (9)$$

In a non-ideal case, the currents, i_{o1+}, i_{o2-} and i_{o3+} are:

$$i_{o1+} = \alpha_3 I_{B1}; i_{o2-} = -\alpha_4 I_{B2}; i_{o3+} = \alpha_5 I_{B3} \ \text{for}\ v_{z-} = V_{DD}$$
$$i_{o1+} = -\alpha_3 I_{B1}; i_{o2-} = \alpha_4 I_{B2}; i_{o3+} = -\alpha_5 I_{B3} \ \text{for}\ v_{z-} = V_{SS} \quad (10)$$

where, α_1, α_2, α_3, α_4 and α_5 are the non-ideal current transfer gains from i_{x+} to i_{z+}, i_{x-} to i_{z-}, I_{B1} to i_{o1+}, I_{B2} to i_{o2-} and I_{B3} to i_{o3+}, respectively; β_1 and β_2 are non-ideal voltage transfer gains from v_y to v_{x+}, and v_y to v_{x-}, respectively; γ_1, γ_2 and γ_3 are transconductance inaccuracies from v_{z-} to i_{o1+}, v_{z-} to i_{o2-} and v_{z-} to i_{o3+}, respectively.

TABLE I
DESCRIPTION SIMULATED VALUES OF PARASITIC COMPONENTS, I.E. THE PARASITIC IMPEDANCES OF DXCCTA

Parasitic	Simulated Values
R_y, C_y	1932x10^{12}Ω, 2.45 fF
R_{x+}	132Ω
R_{x-}	298Ω
R_{z+}, C_{z+}	30.2kΩ, 4.38 fF
R_{z-}, C_{z-}	30.3KΩ, 13 fF
R_{o1+}, C_{o1+}	58.2 KΩ, 3.27fF
R_{o2-}, C_{o2-}	58.2 KΩ, 3.31fF
R_{o3+}, C_{o3+}	58.2 KΩ, 3.35 fF

Furthermore, the various parasitic components, i.e. the parasitic impedances involved in DXCCTA are as follows: three small resistances R_{x+} and R_{x-} appear at $x+$ and $x-$ terminals whereas the parallel combinations of (R_y//(1/sC_y)), (R_{z+}//(1/sC_{z+})), (R_{z-}//(1/sC_{z-})), (R_{o1+}//(1/sC_{o1+})), (R_{o2-}//(1/sC_{o2-})) and (R_{o3+}//(1/C_{o3+})) appear at y, $z+$, $z-$, o_{1+}, o_{2-} and o_{3+} terminals-Fig. 1a, respectively. For the CMOS implementation

of DXCCTA in Fig. 1b, we measured the parasitic impedances of the terminals (using simulation in HSPICE programme), in order to evaluate their effects on processing capabilities of the proposed interface circuits. The values of these parasitic elements are given in Table 1.

Taking the non-idealities and the parasitic impedances into consideration, the proposed conditioning circuit is reanalysed. The amplitude of i_{out} is now modified and given as follows.

$$i_{out} = \begin{cases} \alpha_5 I_{B3} \ for \ v_{z-} = V_{DD} \\ -\alpha_5 I_{B3} \ for \ v_{z-} = V_{SS} \end{cases} \quad (11)$$

The modified threshold levels and peak to peak amplitude are given as

$$V_{HT} = \frac{\alpha_4 I_{B2} R'}{\alpha_1}; V_{LT} = -\frac{\alpha_4 I_{B2} R'}{\alpha_1} \quad (12)$$

$$V_{x+(p-p)} = V_{HT} - V_{LT} = \frac{2\alpha_4 I_{B2} R'}{\alpha_1}$$

where, $R'=R+R_{X+}$. The oscillation frequency is also modified as follows

$$f_o = \frac{1}{T_{ON} + T_{OFF}} = \frac{1}{2R_{sens}\, C' \ln \frac{\alpha_4 I_{B2} R' + \alpha_1 \alpha_3 I_{B1} R_{sens}}{\alpha_1 \alpha_3 I_{B1} R_{sens} - \alpha_4 I_{B2} R'}} \quad (13)$$

where, $C'=C_{sens}+C_{o1+}$. It is observed from (11)-(13) that non-idealities and the parasitic impedances of DXCCTA affect the amplitude of i_{out}, threshold levels, peak to peak amplitude and oscillation frequency, respectively. It is well known that, non-ideal gains deviate from unity only at higher frequencies. Therefore, the effects of these non-idealities could be neglected depending upon the operating frequency range. On the other hand, parasitic effects can be minimized by a proper choice of R and sensor parameters (C_{sens} and R_{sens}). The resistance, R must be selected such that $R>>R_{x+}$ and the capacitor, C_{sens} must be chosen such that $C_{sens}>>C_{o1+}$. Correct selection of the observed parameters leads to improvement in the dynamic range of the sensor circuit, with reduction in the effect of the parasitic components.

In order to further check the performance of the proposed interface circuit, in a situation where there is variation in the fabrication process-the production of semiconductor elements and voltage variation, Monte Carlo simulation (provided by the HSPICE software package itself) was performed in 1000 runs. During this analysis, the voltage supply of ±1.25 V, bias voltage of 0.42V, and bias currents of 50 μA amplitude was used, which resulted in the histogram in Fig. 2. It is assumed that due to possible variation in the manufacturing process, the threshold voltage of all MOS transistors deviates by 5% (Gaussian deviation) and that the variation in the supply voltage (V_{DD} and V_{SS}) is the order of 5% (Gaussian deviation). We assumed that the extreme PVT (Process Voltage Temperature) variations were in the range of +/- 5% (this tolerance is applied over the 0 °C to 100 °C temperature range).

On the basis of such conducted analysis, we are in a position to investigate the effect of the process parameters and the mismatch between transistors on the precision of processing. We define the lower and upper limits of the interval, which contains 95 % of error-absolute value of difference between the predicted and observed output value [20]. The standard deviation in the generated output current input signal was approximately 0.64 μA. It was noted that such changes do not lead to a larger deviation in the frequency of the generated current signal (order of 2%) and that the amplitudes of the output waveforms are not disturbed.

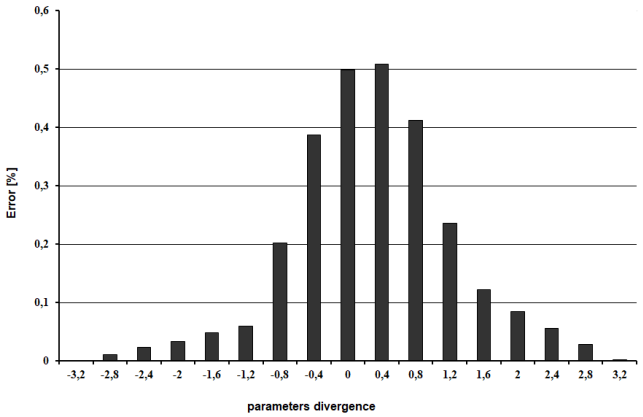

Fig. 2. Distribution of errors in the behaviour of the proposed interface circuit, for divergence in the value of parameters, from their nominal values.

IV. SIMULATION RESULTS

Simulations were performed using HSPICE with 0.18 μm TSMC CMOS process parameters. The supply voltages of ±1.25 V, and bias voltage, V_{BB}=0.42V were used in the simulation. The aspect ratios (*W/L* ratios) of MOS transistors used in the CMOS implementation of DXCCTA are given in Table 2.

TABLE II
MOS TRANSISTOR ASPECT RATIOS (W/L)

M_1-M_2	0.72/0.36
M_3-M_5	1.44/0.36
M_{14}-M_{15}	1.34/0.36
M_{16}-M_{18}	2.4/0.36
M_6-M_{13}, M_{19}-M_{20}	4.8/0.36
M_{21}-M_{26}	1.44/0.36
M_{27}-M_{32}	3.6/0.36

The value of resistance is chosen R=1 kΩ ($R>>R_{X+}$-specified in Table 2). For the specified values of magnitude of i_{out}=50 μA, $v_{C(p-p)}$=100 mV, the values of I_{B1}, I_{B2}, I_{B3} are found according to the design process as follows: $I_{B1}=I_{B2}=I_{B3}$=50 μA and C_{sens}= 500 pF, R_{sens}=4 MΩ. The transient responses of i_{out} and v_C are shown in Fig. 3a. The simulated oscillation frequency of 0.5 MHz is obtained in Fig. 3a, which is similar to the designed oscillation frequency. The transient responses of i_{out} and v_C when I_{B1} is changed to 80 μA are shown in Fig. 3b. The simulated frequency is now changed to 0.789 MHz (1% error) at I_{B1} =80 μA. It can be seen that the threshold levels of v_C and amplitude levels of i_{out} are not affected by the change in bias current, I_{B1}. Fig. 3c shows the electronic tuning of amplitude of i_{out} for different values of I_{B3} (40 μA and 60 μA, I_{B1}=40 μA, I_{B2}=60 μA). It can be seen that the amplitude of i_{out} is independently tunable without affecting the oscillation

frequency.

From the Figs. 3a and 3b we can see that voltage across the sensor possesses a virtually linear characteristic that results from the value of its time constant, which leads to very fast voltage fluctuations in the observed boundaries. Among other things, the proposed conditioning and conversion circuits shows the sensitivity of 8.3×10^{14}Hz/F, which is much better than other circuits used for comparison in Table 1.

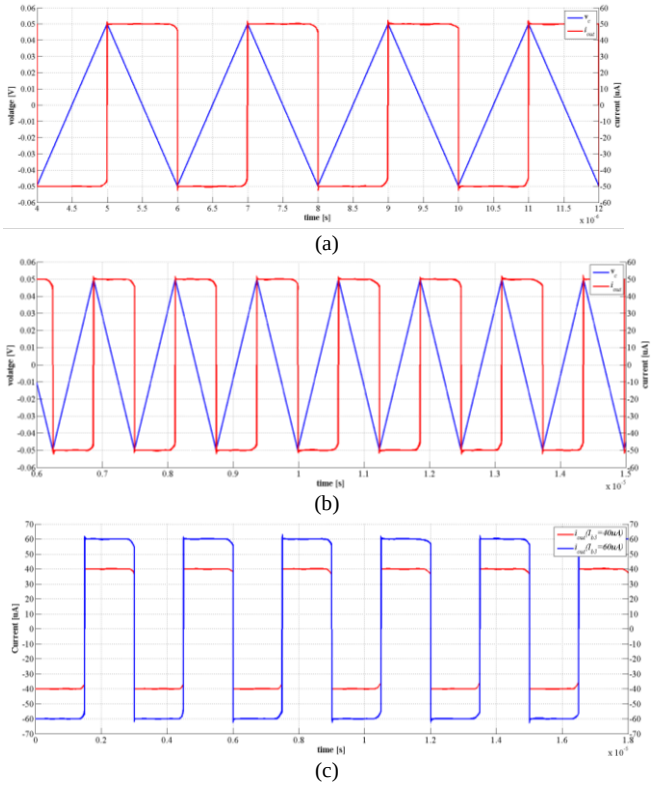

Fig.3. Transient response of proposed interface circuits (a) Simulated waveforms of i_{out} and v_C, $I_{B1}=I_{B2}=I_{B3}=50$ μA, $f_o=0.5$ MHz, (b) simulated waveforms of i_{out} and v_C, $I_{B1}=80$ μA, $I_{B2}=I_{B3}=50$ μA, $f_o=0.789$ MHz, (c) Electronic tuning of amplitude of i_{out} for different values of I_{B3} (40 μA and 60 μA).

For further laboratory and simulation verification of the proposed design we used a JEIO TECH TH-KE-025 temperature and humidity climatic chamber in the relative humidity range 30-90% [11] in which we placed humidity transducer. Prior to each measurement the samples were dried/heated for 20 minutes at 50°C to remove any moisture. The test sample was placed into the chamber and using wires soldered to the electrodes we established connection with acquisition card on our PC and then transferred to the MATLAB environment and after that to HSPICE, without altering to plot the curves. The humidity was varied between 30 and 90% at 25°C, by setting the desired humidity value. The simulation observed in this way (with input data obtained on real humidity transducer), waveforms of i_{out} and v_{x+} are shown in Fig. 4 - the response in the time domain of the proposed sensor system in a situation where the environmental humidity is changed. The simulation oscillation frequency in situation when moisture is 60%RH is 0.1542 MHz (0.58% error in comparison with calculated frequency). The electronic tuning of amplitude of i_{out} via bias current $I_{B3}=250$ μA is shown in Fig. 4c, which shows that the amplitude of i_{out} can be independently controlled without disturbing the oscillation frequency.

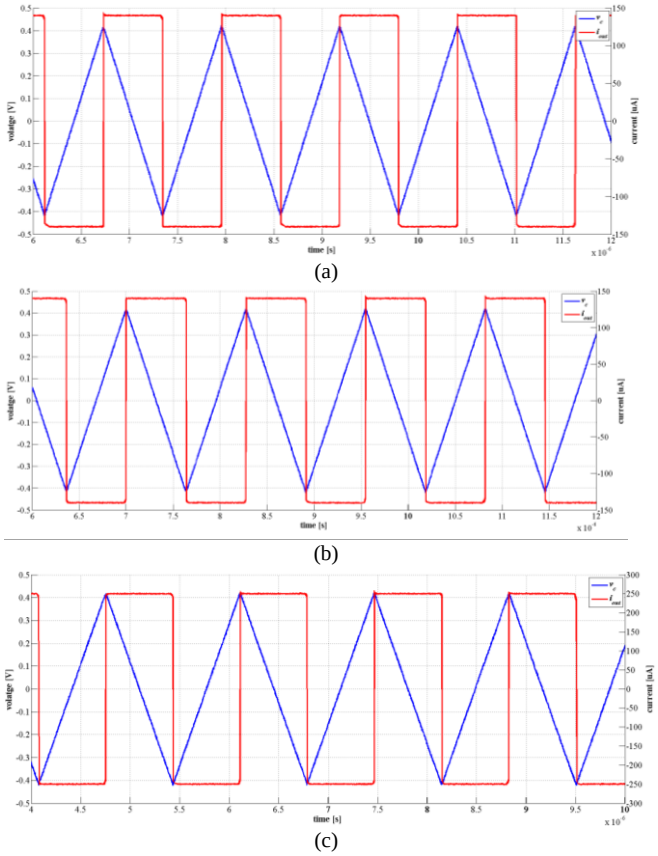

Fig.4. The time domain behaviour of the proposed interface circuits (a) 30%RH, (b) 60%RH, (c) 90%RH and bias current $I_{B3}=250$ μA.

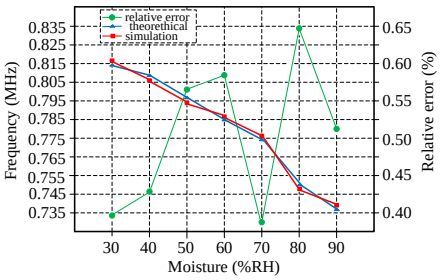

Fig.5. Features of the proposed interface circuits-change in the frequency of the output signal with moisture concentration and difference (error) between theorethical data and expectation-simulation results (theory versus simulation measurement).

Using the MATLAB environment we detected the frequency of the output current signal and subsequent signal conditioning (on external resistance connected to the input pin of the acquisition card to obtain a voltage equivalent). To count input edges of the square wave output signal, the timer as a counter has been used. The dependence of the frequency f of the output current signal on the humidity of the environment in which the sensor circuit is located (the chamber used during the laboratory performance test of the proposed sensor system) is shown in Fig. 5. It shows that the frequency is proportional to

the capacitance change with moisture content. On the same Fig. 5, we compared the simulation and theoretical measurement results. We can see that the obtained results are well correlated because the error (relative) in the operating range of 30% to 90% RH is below 0.65%. The proposed sensor system possesses satisfactory properties in terms of error and gives a linear frequency change relationship.

The response time of a sensor when exposed to moisture is defined as the time in which a sensor reaches 90% of the total response, while recovery is the time required for a sensor to return to 90% of the original baseline signal, when moisture is removed [11]. The average response time was about 16s, while the recovery time was very fast and the sensor recovered in 1s. The difference in response and recovery times was attributed to the microstructure of pseudobrookite thick films that represented a porous network of aggregated nanoparticles [11].

V. CONCLUSION

In this paper, a humidity sensor read out circuitry using DXCCTA has been designed. The proposed interface provides a simple interconnection with the associated processing unit without post-processing, with very low power consumption of 1mW. It is important to note that the proposed design can be fully realized in the form of an integrated circuit. The proposed solution is based on generating a fully autonomous current signal, the period of which is linearly dependent on the capacity of the humidity sensor. The possibility of precise humidity measurement in the range of 30% to 90% RH with error less than 1.5% was experimentally confirmed (sensitivity 8.3 x1014Hz/F over the full range of changes). The design can be used for a humidity sensor and can be adopted by industries due to its flexibility in design that could be beneficial from the point of view of industrial production costs.

REFERENCES

[1] F. Reverter, O. Casas, "Direct interface circuit for capacitive humidity sensors", Sensors and Actuators A, 2008, 143, 315–322.

[2] B. George, et al. (eds.), *Advanced Interfacing Techniques for Sensors*, Smart Sensors', Measurement and Instrumentation, 2017, 25. DOI: 10.1007/978-3-319-55369-6_2.

[3] N. Kuriyal, R. Kumar, V. Ramola, "Optimization and Simulation of humidity sensor readout circuitry using two stage op amp", IOSR Journal of Electrical and Electronics Engineering, 2014, 9 (5), 66-72.

[4] T. Jalkanen, A. Määttänen, E. Mäkilä, J. Tuura, M. Kaasalainen, V.P. Lehto, P. Ihalainen, J. Peltonen, J. Salonen, "Fabrication of Porous Silicon Based Humidity Sensing Elements on Paper", Journal of Sensors, 2015, Article ID 927396, 10 pages. DOI:10.1155/2015/927396.

[5] O. Nizhnik, K. Higuchi, K. Maenaka: "A Standard CMOS Humidity Sensor without Post-Processing", Sensors, 2011, 11, 6197-6202. DOI:10.3390/s110606197.

[6] P. Nath, I. Hussain, S. Dutta, A. Choudhury, "Solvent treated paper resistor for filter circuit operation and relative humidity sensing", Indian Journal of Physics, 2014, 88 (10), 1093-1097. DOI: 10.1007/s12648-014-0547-x.

[7] T.A. Blank, L.P. Eksperiandorova, K.N. Belikov, "Recent trends of ceramic humidity sensors development", Sensors and Actuators B, 2016, 228, 416-442.

[8] A. Urrutia, J. Goicoechea, A.L. Ricchiuti, V.D. Barrera, M.S. Sales, F.J. Arregui, "Simultaneous measurement of humidity and temperature based on a partially coated optical fiber long period grating", Sensors and Actuators B: Chemical, 2016, 227, 135-141.

[9] A. Mirzaei, B. Hashemi, K. Janghorban, "-Fe2O3 based nanomaterials as gas sensors", J. Mater. Sci.: Mater. Electron., 2016, 27, 3109-3144.

[10] G. Miskovic, M.D. Lukovic, M,V. Nikolic, Z.Z. Vasiljevic, J. Nicolics, O.S. Aleksic, "Analysis of electronic properties of pseudobrookite thick films with a possible application for NO gas sensing", Proceedings of the 39th International Spring Seminar on Electronics Technology, 2016, 386-391.

[11] M.V. Nikolic, Z.Z. Vasiljevic, M.D. Lukovic, V.P. Pavlovic, J. Vujancevic, M. Radovanovic, J.B. Krstic, B. Vlahovic, V.B. Pavlovic, "Humidity sensing properties of nanocrystalline pseudobrookite (Fe2TiO5) based thick films", Sensors and Actuators B: Chemical, 2018, 277, 654-664. DOI: 10.1016/j.snb.2018.09.063.

[12] L. Polak, R. Sotner, J. Petrzela, J. Jerabek, "CMOS Current Feedback Operational Amplifier-Based Relaxation Generator for Capacity to Voltage Sensor Interface, Sensors", 2018, 18 (4488), 15 pages. DOI:10.3390/s18124488.

[13] T. Islam, S.C. Mukhopadhyay, N.K Suryadevara, "Smart Sensors and Internet of Things", A Postgraduate Paper, IEEE Sensors Journal, 2017, 17 (3), 577 – 584.

[14] T. Ameloot, P.V. Torre, H. Rogier, "A Compact Low-Power LoRa IoT Sensor Node with Extended Dynamic Range for Channel Measurements", Sensors, 2018, 18 (2173), 1-16. DOI:10.3390/s18072137.

[15] Microchip PIC 16(L)F19155, Microchip Technology Inc., USA, 2017.

[16] A. Kumar, B. Chaturvedi, "Novel CMOS dual-X current conveyor transconductance amplifier realization with current-mode multifunction filter and quadrature oscillator", Circuits, Systems and Signal Processing, 2018, 37, 2250-2277.

[17] A.U. Khan, T. Islam, J. Akhtar, "An Oscillator-Based Active Bridge Circuit for Interfacing Capacitive Sensors With Microcontroller Compatibility", IEEE Trans. Instrum. Meas., 2016, 65 (11), 2560 – 2568.

[18] A.D. Amico, C.D. Natale, "A contribution on some basic definitions of sensors properties", IEEE Sensors J., 2001, 1 (3), 183–190.

[19] G.F. Fine, L.M. Cavanagh, A. Afonja, R. Binions, "Metal oxide semi-conductor gas sensors in environmental monitoring", Sensors, 2010, 10, 5469-5502. DOI: 10.3390/s10060546

[20] Evaluation of measurement data. Supplement 1 to the "*Guide to the expression of uncertainty in measurement*" - Propagation of distributions using a Monte Carlo method, BIPM, 2008.

[21] Shaw Automatic Dewpoint Meter Data Manual, SHAW Moisture Meters Ltd., Bradford, U.K., 2004.